Pathways of the water masses exiting the Labrador Sea

The importance of boundary–interior exchanges

Georgiou, Sotiria; Ypma, Stefanie L.; Brüggemann, Nils; Sayol, Juan Manuel; Pietrzak, Julie D.; Katsman, Caroline A.

DOI
10.1016/j.ocemod.2020.101623

Publication date
2020

Document Version
Final published version

Published in
Ocean Modelling

Ocean Modelling 150 (2020) 101623

Contents lists available at ScienceDirect

Ocean Modelling

journal homepage: www.elsevier.com/locate/ocemod

Pathways of the water masses exiting the Labrador Sea: The importance of boundary–interior exchanges

Sotiria Georgiou [a,*], Stefanie L. Ypma [a], Nils Brüggemann [b], Juan-Manuel Sayol [a], Julie D. Pietrzak [a], Caroline A. Katsman [a]

[a] Section of Environmental Fluid Mechanics, Faculty of Civil Engineering and Geosciences, Delft University of Technology, Delft, The Netherlands
[b] Faculty of Mathematics, Informatics and Natural Sciences, University of Hamburg, Hamburg, Germany

ARTICLE INFO

Keywords:
Labrador Sea Water export
Convection
Labrador Sea
Atlantic Meridional Overturning Circulation
Lagrangian
Pathways

ABSTRACT

The water masses exiting the Labrador Sea, and in particular the dense water mass formed by convection (i.e. Labrador Sea Water, LSW), are important components of the Atlantic Meridional Overturning Circulation (AMOC). Several studies have questioned the connection of the LSW production to the AMOC variability. This is partly due to the limited understanding of how this locally formed water mass leaves the interior of the Labrador Sea. In this study, the pathways and the timescales of the water masses exiting the Labrador Sea via the boundary current are investigated by Lagrangian particle tracking. This method is applied to the output of a strongly-eddying idealized model that is capable of representing the essential physical processes involved in the cycle of convection and restratification in the Labrador Sea. The Lagrangian trajectories reveal that prior to exiting the domain the water masses follow either a fast route within the boundary current or a slower route that involves boundary current-interior exchanges. The densest water masses exiting the Labrador Sea stem from this slow route, where particles experience strong water mass transformation while in the interior. In contrast, the particles that follow the fast route experience water mass transformation in the boundary current at the western side of the domain only, yielding a lighter product. Although both routes carry roughly the same transport, we show that 60% of the overturning in density space is associated with the volume transport carried by particles that follow the slow route. This study further highlights that the export of dense water masses, which is governed by the eddy activity in the basin, yields export timescales that are usually longer than a year. This underlines the necessity of resolving the mesoscale features required to capture the interior–boundary current exchange in order to correctly represent the export of the LSW.

1. Introduction

The Atlantic Meridional Overturning Circulation (AMOC) describes the conversion of lighter, shallow Atlantic water masses flowing northward into denser, deep water masses flowing southward, involving diabatic processes like deep convection in the marginal seas of the North Atlantic. The strength of the AMOC is commonly estimated as the total northward transport in the upper 1000m or so of the water column and can be either viewed in depth space, emphasizing the vertical transport (Wunsch and Heimbach, 2006; Cunningham et al., 2007) or in density space emphasizing the transformation of lighter to denser water masses (e.g., Xu et al., 2016; Li et al., 2017; Desbruyères et al., 2019; Lozier et al., 2019; Brüggemann and Katsman, 2019). Climate model studies suggest a substantial weakening of the AMOC over the 21st century (Collins et al., 2013; Weijer et al., 2019), with the potential to affect the global climate. Therefore, over the last decade, there has been an increased effort to understand the drivers of AMOC variability (e.g., Johnson et al., 2019; Lozier et al., 2019).

One of these potential drivers is the process of deep convection in the Labrador Sea, resulting in the production of Labrador Sea Water (LSW); one of the water masses that contribute to the lower limb of the AMOC (e.g., Rhein et al., 2017). While earlier modeling studies have suggested a close connection between the LSW production and AMOC variability (Biastoch et al., 2008; Zhang, 2010; Yeager and Danabasoglu, 2014), up-to-date observations at the RAPID 26°N (Smeed et al., 2018) and OSNAP (Lozier et al., 2019) arrays and recent numerical studies (Zou and Lozier, 2016; Li and Lozier, 2018; Georgiou et al., 2019) have cast doubts on this, suggesting a rather complex connection between the two. Moreover, the recent study of Lozier et al. (2019) suggests that the variability of the overturning is dominated by the water mass transformation taking place in the eastern half of subpolar gyre rather than in the Labrador Sea.

* Correspondence to: Environmental Fluid Mechanics, Stevingweg 1, 2628 CN, Delft, The Netherlands.
E-mail address: S.Georgiou@tudelft.nl (S. Georgiou).

https://doi.org/10.1016/j.ocemod.2020.101623
Received 7 November 2019; Received in revised form 26 March 2020; Accepted 1 April 2020
Available online 3 April 2020

The recent debate on the importance of the LSW for AMOC variability is partly the result of limited understanding on how this water mass leaves the interior of the Labrador Sea, in particular about its export routes and the associated timescales. Several studies showed that newly-formed LSW is rapidly exported by spreading laterally and entraining in the Deep Western Boundary Current (DWBC) near the Labrador coast (e.g., Talley and McCartney, 1982; Brandt et al., 2007; Feucher et al., 2019). Moreover, a mid-depth recirculation of the LSW within the subpolar gyre has been reported in a number of studies (e.g., Lavender et al., 2000; Pickart et al., 2003; Stramma et al., 2004; Bower et al., 2009; Holliday et al., 2009; Lozier et al., 2013). Last, a slower export route has been suggested in the studies of Straneo et al. (2003) and Palter et al. (2008). In particular, they identify the existence of a pathway which transports convected water from the interior towards the West coast of Greenland. These multiple export routes of LSW, of which the relative importance is still unclear, might result in a complex relation between the LSW formation and its export timescales, and the AMOC variability.

The recent highly idealized numerical study of a convective marginal sea by Brüggemann and Katsman (2019) clearly highlights the important role of the exchange of waters between the interior and the boundary current, which in turn is governed by the eddy activity, for the export pathways of convected water and the associated timescales. Their results indicated that the densest water masses are formed in the interior and are laterally steered towards the region of high eddy activity and then entrained in the boundary current, thus following an indirect route to leave the marginal sea. In addition, they showed that a lighter product of convection within the boundary current itself is directly and rapidly exported via that boundary current. The underlying idea of an eddy-induced entrainment of LSW in the boundary current was pointed out by Khatiwala and Visbeck (2000). However, they linked this entrainment to the summertime restratification process and the associated horizontal density gradients. That is, they assumed no spatial variations and by linking it to the restratification implied that this only occurs in summer. In contrast, both Brüggemann and Katsman (2019) and Georgiou et al. (2019), show that there is a preferred region for the re-entrainment, which coincides with the region where the eddy activity peaks. However, both studies conclude this based on an analysis of passive tracers, which does not allow the investigation of the pathways and transformation of water masses, which in the end determine the LSW export.

The direct and indirect export routes of the convected water recently identified in idealized models (Brüggemann and Katsman, 2019; Georgiou et al., 2019) are in line with the indications of such routes from observations (e.g., Palter et al., 2008; Bower et al., 2009). However, due to the limited number of observations, the relative importance of a direct export route on the Labrador side of the basin and an indirect route via the Greenland coast is yet unclear.

In this study, we analyze the origin and transformation of different water masses found within the boundary current at the exit of the Labrador Sea. We use a Lagrangian approach applied to the output from the idealized model used in Georgiou et al. (2019), which allows us to elucidate the complex structure of the flow (Bower et al., 2019). From this we distinguish different pathways, identify where water mass transformation occurs and assess what role the prominent eddy field plays for exporting these water masses. This idealized model study provides helpful insights on the nature of the interior–boundary current exchange and its role for the LSW export. The results can guide the analyses of observations and more realistic model simulations, thus improving our overall understanding in AMOC.

The structure of this paper is as follows. The model setup and the Lagrangian approach are described in Section 2. First, the pathways that the water masses follow before exiting the Labrador Sea are analyzed in Section 3. Next, we explore the importance of each pathway for the net overturning in depth and density space (Section 4) and the location where the water masses subduct (Section 5). In Section 6, we focus on the lateral exchange between the boundary current and the interior by identifying the locations where this exchange occurs and how it affects the properties of the water masses exiting the Labrador Sea. The associated export timescales are addressed in Section 7, followed by a discussion and conclusions in Section 8.

2. Numerical model and methods

2.1. Model configuration and flow characteristics

The numerical simulation analyzed in this study is carried out using a hydrostatic configuration of the MITgcm (Marshall et al., 1997). The model configuration captures the key features of the circulation in the Labrador Sea, like the annual cycle of the convection and restratification and the properties of the mesoscale eddy field. This model and its results have been previously used in Georgiou et al. (2019) and we refer the reader to this study for a more detailed description of the model setup.

The model has a horizontal resolution of 3.75 km and 40 levels in the vertical with a resolution of 20 m in the upper layers up to 200 m at a maximum depth of 3000 m. The model domain has two open boundaries (each roughly 100 km wide), one in the northeast and one in the southwest, where a boundary current enters and exits the domain. All other boundaries are closed (Fig. 1). At the northeastern open boundary, a warm boundary current is specified by a meridional temperature field $T_{in}(y, z)$ and a westward flow $U_{in}(y, z)$ in geostrophic balance with this prescribed temperature distribution. A sinusoidal seasonally varying term is added to the inflow conditions to mimic the observed seasonal variability of the West Greenland Current (ΔU_{max} = 0.4 m s^{-1}, with maximum and minimum in September and March respectively, Kulan and Myers, 2009; Rykova et al., 2015). Note that total outflow transport is prescribed, but the properties of the boundary current at the outflow are determined by the internal model dynamics. Following the topography, this boundary current flows cyclonically around the basin (Fig. 1a). At the northwestern side, a narrowing of the topography is present (gray contours in Fig. 1a) as observed near the west coast of Greenland. This steepening leads to an increased instability of the boundary current and mostly warm anticyclonic eddies are shed, with similar characteristics as the Irminger Rings (IRs) as shown in Katsman et al. (2004), Gelderloos et al. (2011) and Georgiou et al. (2019). At the surface, a temporally and spatially varying surface heat flux is applied resulting in a net annual heat loss of 18 W m^{-2} over the entire model domain (blue contours in Fig. 1b, see Georgiou et al. (2019) for details).

A linear equation of state is used, with temperature as the only active tracer. Note that the effects of salinity are not incorporated in the model although in reality the lateral fresh water flux carried by the IRs (e.g., de Jong et al., 2016) influences the properties of convection (e.g., Gelderloos et al., 2012). In this study our focus is on the dynamics that control the interior–boundary current exchange in the Labrador Sea, and hence the effects of salinity are omitted in the model for simplicity.

As a result of the applied surface heat loss (blue contours in Fig. 1b) the model displays deep convection in the interior. The winter mean mixed layer reaches a depth of 1700 m (Fig. 1b). As shown in Georgiou et al. (2019), the deepest mixed layers are located away from areas with strong eddy activity (red contours in Fig. 1b) albeit slightly closer to the maximum of buoyancy loss than observed. In the regions of strong eddy activity the associated eddy heat transport from the boundary current towards the interior is stronger and the water column is too stratified to sustain deep convection. In the model we do not consider the shelf and overflow waters or the effects of wind (Gelderloos et al., 2011), and prescribe a transport at the inflow (19.7 Sv) that is weaker than estimates over the full depth (40–50 Sv, Pickart et al., 2002; Fischer et al., 2004). The maximum barotropic streamfunction is about 27 Sv (Fig. 1c) due to some recirculation in the basin. In this study, we use the three dimensional velocity field from the last six years of the reference simulation (i.e. model years 15–20) described in Georgiou et al. (2019) to track Lagrangian particles.

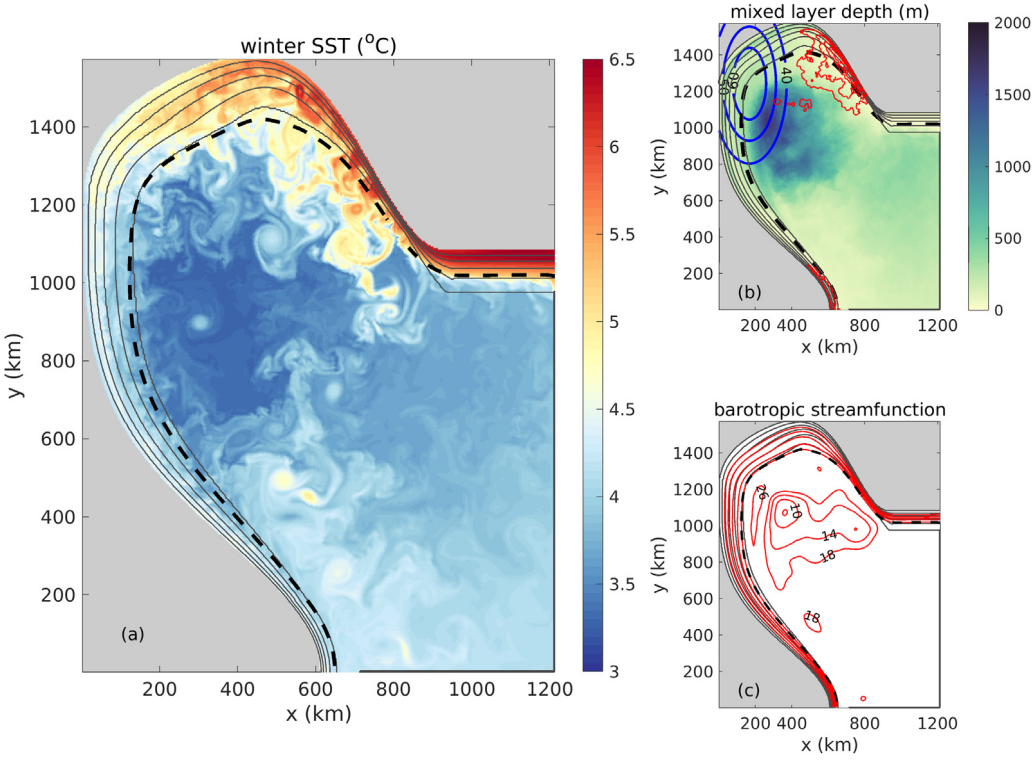

Fig. 1. (a) Snapshot of the sea surface temperature (SST) in mid-March of model year 16. (b) Winter (February–March) mixed layer depth (MLD in m, shading), eddy kinetic energy (EKE, red contours, contour interval is 200 $cm^2\ s^{-2}$) and annual mean surface heat flux (contours in blue, contour interval is 10 $W\ m^{-2}$). (c) Mean barotropic streamfunction (Ψ_b, contour interval is 4 Sv). All model data are from the reference simulation described in Georgiou et al. (2019); values in (b) and (c) are averaged over years 16–20. In all figures, black dashed line indicates the 18 Sv contour line of Ψ_b and gray contours outline the bathymetry (contour interval is 500 m starting from the isobath of 500 m).

2.2. Lagrangian particle tracking

The offline Lagrangian tool Connectivity Modeling System (CMS, Paris et al., 2013) is used to investigate the possible pathways of the waters exiting the model domain and water mass transformation that occurs along these pathways. To this end, numerical particles are released at the outflow region in the south (the only export route of the convected water mass out of the domain). The particles are advected backward in time using a timestep of 1 h within the 2-day snapshots of the three dimensional velocity fields of the simulation described in the previous section. The movement of the numerical particles is parameterized as described by Paris et al. (2013): a Runge–Kutta 4th order stepping in time and a tricubic spatial interpolation are used to determine the location of the particles; no additional horizontal diffusivity is applied. To account for the increased vertical diffusion during the process of convection, particles that are located within the mixed layer are moved randomly in the vertical within the mixed layer with a maximum velocity of w = 10 cm s^{-1} (van Sebille et al., 2013).

Particles are released at the outflow (y = 3.75 km, red line in Fig. 2a) every 2 days over a period of one year with a particle resolution of 1 km in the zonal direction and 50 m vertically. Doing so, we track 217349 Lagrangian particles over a period of 6 years. Since we are interested in distinguishing the pathways of the water masses in terms of volume transport, a volume transport is assigned to each particle upon release and it is conserved along the trajectory (van Sebille et al., 2018). This is determined by multiplying the meridional velocity by the area of the grid cell in which the particle is released (Döös, 1995; Ypma et al., 2019). Although the particles were released at the outflow and tracked backwards, we will mostly refer to their trajectories forward in time.

3. Pathways and origin of the water masses exiting the Labrador Sea

In this study, we explore the origin of the waters found in the boundary current at the outflow of the Labrador Sea. In particular, we investigate the role of exchange water between the boundary current and the interior. To this end, we define a particle as being in the interior when it is offshore of the 18 Sv contour line of the 5-year mean barotropic streamfunction (Ψ_b, black dashed line in Figs. 1 and 2a). To filter out possible short and fast excursions of particles into the interior and back, we also require that the particle stays offshore of this streamline for more than 20 days. The results of the analyses presented in this study are not very sensitive to the exact choice made for distinguishing the boundary current from the interior: the presented results are consistent for different choices of Ψ_b or using an isobath.

Within the 6 year advection time, 90% of the particles (i.e. 195528 particles) reach the eastern open boundary (inflow). Since these particles travel from the inflow towards the outflow we will refer to them as *wholeLoop* particles. The 10% of the particles that remain in the basin during the 6 year simulation are referred to as *interiorLong* particles.

A particle density plot (Fig. 2a) highlights the paths that the *wholeLoop* and *interiorLong* particles are prone to follow. It is constructed by regridding the position of each particle at every timestep on an x-y grid with a resolution of 3.75 km. This particle density is calculated as described in Ypma et al. (2019); at each location (in the new grid) the transport assigned to each particle is divided by the total transport carried by the particles. In the interior, the particle density is enhanced at the northwestern side of the basin (close to the topographic narrowing, Fig. 2a). This indicates that a significant number of particles enter the interior of the basin there, suggesting a connection with the eddy activity found at this location (Fig. 1b). However, such a possible connection is masked by the fact that the highest particle

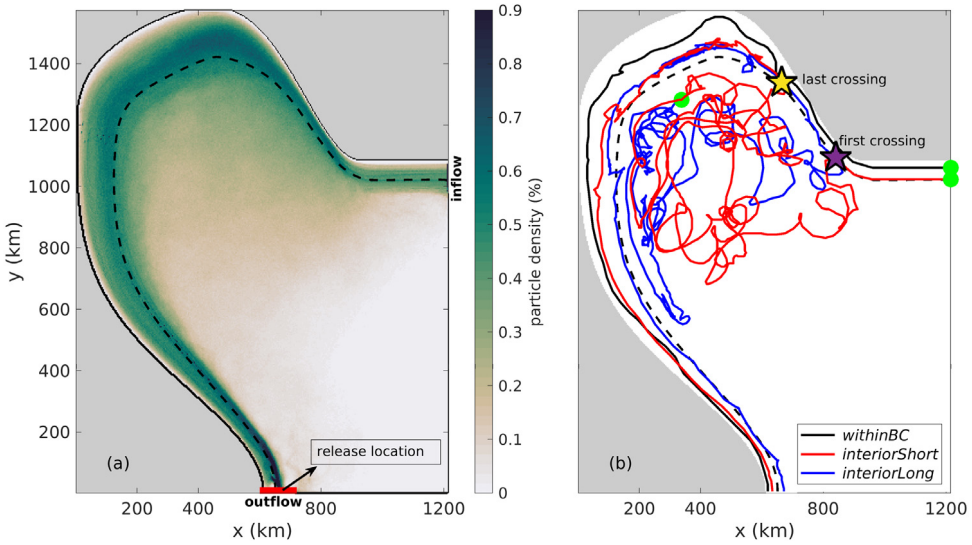

Fig. 2. (a) Density of the position of particles released at y = 3.75 km (red line). The black dashed line shows the 18 Sv barotropic streamfunction (Ψ_b) which is used to distinguish the boundary current from the interior. (b) Example trajectories of a particle following the boundary current (*withinBC*, black line), a particle crossing into the interior (*interiorShort*, red line) and a particle that does not leave the basin during the 6-year simulation (*interiorLong*, blue line). The purple (yellow) star indicates the location where the example *interiorShort* particle crosses the 18 Sv barotropic streamfunction (dashed line) for the first (last) time. Green circles indicate the location of the particles at the end of the backward advection time (i.e. at t = 6 years).

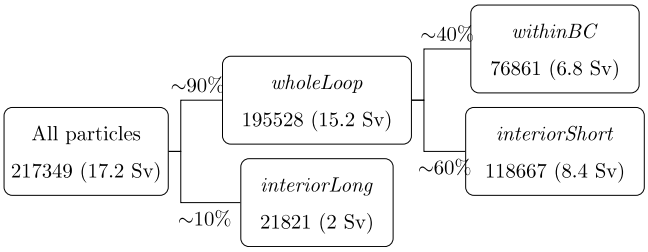

Fig. 3. Schematic showing the number, percentage and associated volume transport of particles that fall into various categories; *wholeLoop* particles travel from the inflow towards the outflow, *interiorShort* particles cross the 18 Sv contour line of Ψ_b into the interior and back, *withinBC* particles never leave the boundary current. Last, *interiorLong* particles remain in the basin during the 6 year simulation. Examples of pathway for *withinBC*, *interiorShort* and *interiorLong* are shown in Fig. 2b.

density occurs along the boundary current, which suggests that the particles are found somewhere within the boundary current during their lifetime. We therefore subdivide the *wholeLoop* particles in two groups: particles that cross the 18 Sv contour line of Ψ_b into the interior at some location (hereinafter, *interiorShort* particles) and particles that never cross the 18 Sv contour line and thus never leave the boundary current (hereinafter, *withinBC* particles). It appears that of all the *wholeLoop* particles, 60% falls into the *interiorShort* category and 40% in the *withinBC* category (Fig. 3). The volume transport carried by the *withinBC*, *interiorShort* and *interiorLong* particles amounts to 6.8 Sv, 8.4 Sv and 2.0 Sv, respectively (Fig. 3). Note that at the eastern side of the domain (x > 800 km and y < 1000 km) the particle density is low (<1%, Fig. 2a). This reflects the weak circulation in this part of the domain (Fig. 1c). This is a consequence of the closed southeastern boundary of the idealized model. The bathymetry forces the boundary current to follow the northern and western side of the domain.

By construction, the *withinBC* particles (black line in Fig. 2b) are always onshore of the 18 Sv contour line of Ψ_b. The *interiorShort* particles (red line in Fig. 2b) also travel from the inflow to the outflow but along their path, they enter the interior (purple star in Fig. 2b) and re-enter the boundary current (yellow star in Fig. 2b) before exiting the domain. Last, the *interiorLong* particles recirculate in the interior of the basin for more than 6 years (blue line in Fig. 2b).

Most of the *withinBC* particles reside close to the lateral boundaries at both the inflow and the outflow (black contours in Fig. 4). The particles that enter the interior and leave the domain within the simulated advection time (*interiorShort*, red contours in Fig. 4) originate farther offshore (y = 1020–1060 km) than the *withinBC* particles (y = 1040–1080 km, Fig. 4b). Since they are at the flank of the boundary current at the inflow (Fig. 4b), they can more easily leave the boundary current and enter the interior. Similarly, when they re-enter the boundary current, they are found on its offshore flank (Fig. 4a), but deeper in the water column. Last, the *interiorLong* particles are found in the deepest part of the boundary current (blue contours in Fig. 4a). Apparently, they represent the densest water masses exiting the domain.

4. Overturning in depth and density space

The particles that represent the three pathways of water masses prior to exiting the Labrador Sea display a depth change (Fig. 4), which is a reflection of overturning in depth space in the basin. Moreover, using the same model setup, it is shown from an Eulerian perspective that the boundary current gets denser along its path through the Labrador Sea, yielding a net overturning in density space (Georgiou et al., 2019). In this section, we analyze this overturning both in depth and density space from a Lagrangian perspective and investigate the relative contribution of the different pathways to this net overturning.

4.1. Transport changes between the inflow and outflow in depth space

Since each of the particles represents a particular transport of water masses (Section 2.2), we can convert the depth changes of particles between inflow (green bars) and outflow (orange bars) to the associated volume transport (Fig. 5). Three vertical layers are defined to facilitate discussion; 0–500 m, 500–1500 m and 1500–3000 m (black horizontal lines in Fig. 5a–c). At the inflow, almost all transport carried by either the *withinBC* or the *interiorShort* particles, is found shallower than 1500 m (6.8 Sv and 8.2 Sv respectively). This view changes at the outflow of the domain: the volume transport in the deepest layer (1500–3000 m) increases by 1.3 Sv for the *withinBC* and by 2.0 Sv for the *interiorShort* particles. In addition, the presence of the *interiorLong* particles at the outflow becomes apparent in this depth layer as a volume transport of 1.8 Sv (90% of the total transport these particles represent).

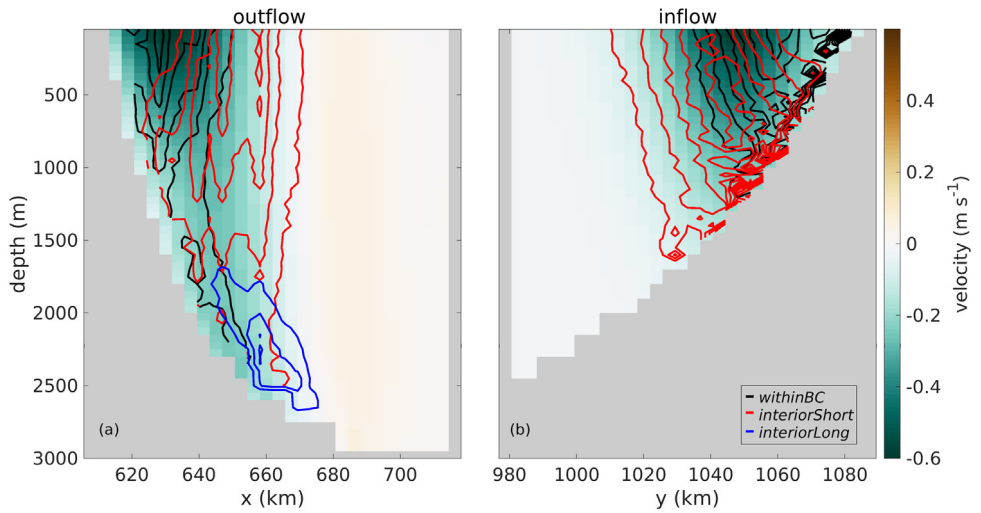

Fig. 4. Section across (a) the outflow (at y = 3.75 km) and (b) the inflow (at x = 1215 km) showing the number of Lagrangian particles that follow the three pathways: *withinBC* (black contours), *interiorShort* (red contours) and *interiorLong* (blue contours) together with the 5 year mean velocity of the simulation (shading). The contour interval is 100 particles.

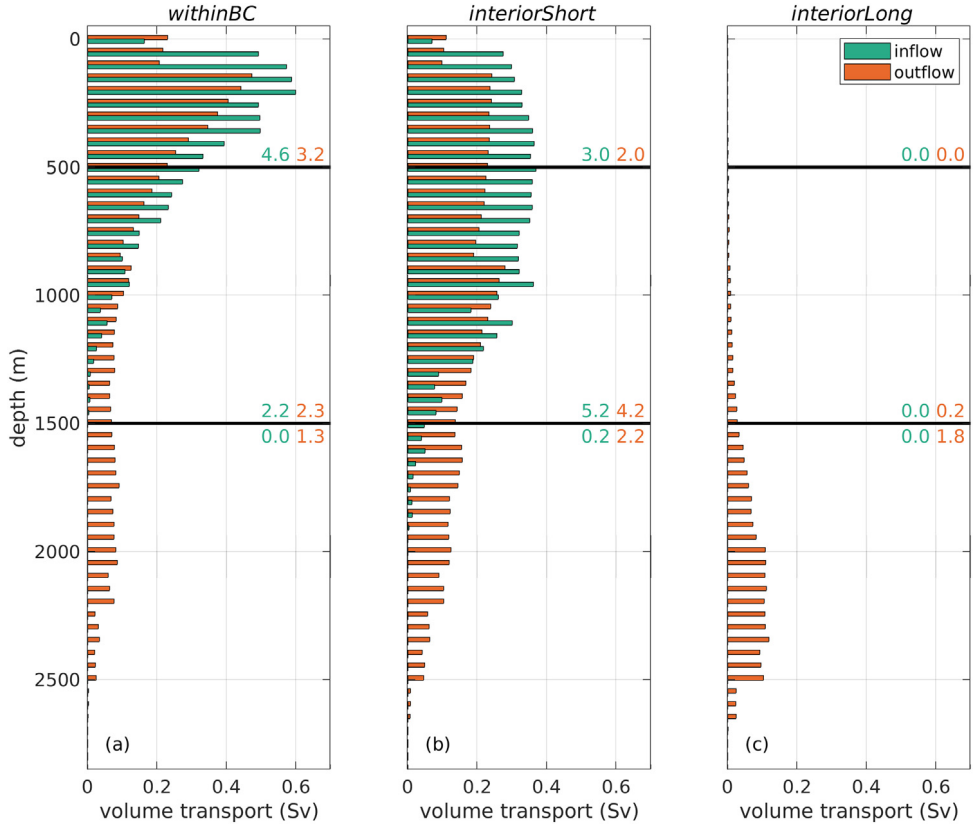

Fig. 5. Volume transport (in Sv) at the inflow (green bars) and outflow (orange bars) binned every 50 m in depth space for the particle categories (a) *withinBC*, (b) *interiorShort* and (c) *interiorLong*. Black horizontal lines distinguish (a–c) three depth layers (0–500 m, 500–1500 m and 1500–3000 m); the values in green (orange) represent the total transport in each layer at the inflow (outflow).

4.2. Transport changes between the inflow and outflow in density space

Similarly, we can explore the water mass transformation that occurs between inflow and outflow from a Lagrangian perspective. Since the density in the model is associated only with temperature variations (Section 2.1), we examine the temperature changes between inflow and outflow for each pathway. At the inflow, most of the *withinBC* particles carry warm water masses (green bars in Fig. 6a). A shift in transport of warmer to colder water masses between inflow and outflow reveals that water mass transformation occurs within the boundary current. Since the *interiorShort* particles originate farther offshore in the boundary current (Fig. 4b), they are characterized by lower temperatures at the

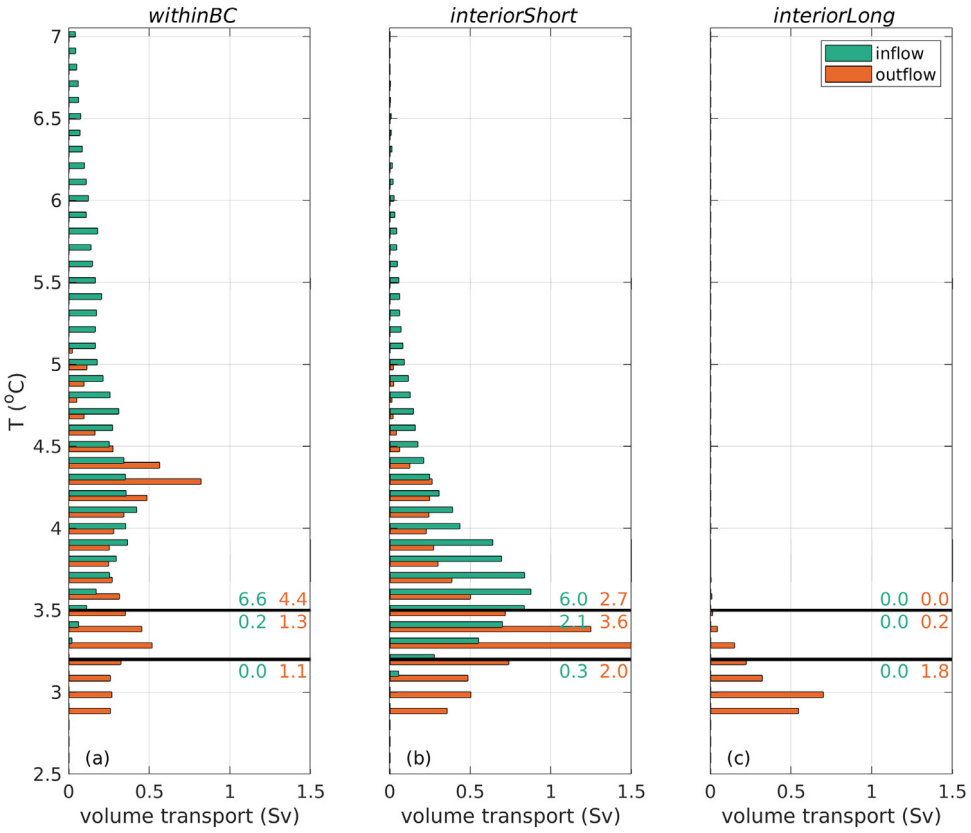

Fig. 6. Volume transport (in Sv) at the inflow (green bars) and outflow (orange bars) binned every 0.1 °C in temperature space for the particle categories (a) *withinBC*, (b) *interiorShort* and (c) *interiorLong*. Black horizontal lines distinguish three water mass definitions: surface waters ($T > 3.5$ °C), intermediate waters ($3.2 < T \leqslant 3.5$ °C) and deep waters ($T \leqslant 3.2$ °C); the values in green (orange) represent the total transport for each water mass at the inflow (outflow). Note that the intermediate waters correspond to the temperature range of the convected water mass (Georgiou et al., 2019).

inflow (green bars in Fig. 6b). Also for this category, the transport in colder layers increases towards the outflow indicating that the particles experience water mass transformation along their path. Last, the *interiorLong* particles represent the coldest water masses at the outflow (Fig. 6c).

To quantify the water mass transformation in density space, the total volume transport at the inflow (outflow) is summarized in Fig. 6 for three water mass definitions: surface waters ($T > 3.5$ °C), intermediate waters ($3.2 < T \leqslant 3.5$ °C) and deep waters ($T \leqslant 3.2$ °C). Note that T = 3.2–3.5 °C is the temperature range corresponding to the convected water mass (Georgiou et al., 2019). The transport change between inflow and outflow in temperature space through the 3.5 °C isotherm derived from the particles amounts to $(1.3 + 1.1) - 0.2 = 2.2$ Sv for *withinBC* (Fig. 6a) and to $(3.6+2.2)-(2.1+0.3) = 3.4$ Sv for *interiorShort* (Fig. 6b). Furthermore, the transport of water masses below 3.5 °C at the outflow is substantially higher for both the *interiorShort* and *interiorLong* particles (7.6 Sv combined, Fig. 6b–c) than for the *withinBC* (2.4 Sv, Fig. 6a).

4.3. Overturning from the Eulerian and the Lagrangian perspective

Based on Figs. 5 and 6, we can estimate the overturning in both depth and density space and compare this to the overturning calculated from the Eulerian velocities. The Eulerian overturning in depth space is defined as the difference in time-mean transport between the inflow and the outflow in model year 15, integrated over the same depth bins (depth space) or temperature bins (density space). Next, we calculate the Lagrangian overturning for each pathway, by taking the difference between the summed volume transport carried by all particles in a certain depth or density bin at the outflow and at the inflow. This is done for all three particle categories. Since the *interiorLong* particles never reach the inflow, the total mean Lagrangian overturning estimate is based solely on the transports carried by the *withinBC* and *interiorShort* particles. We do not expect the Eulerian and Lagrangian overturning estimates to match exactly as we lack information on the overturning associated with the *interiorLong* particles since we cannot follow them backwards in time towards the inflow.

However, the overturning derived from the particles largely agrees with the overturning obtained from the time mean Eulerian flow (compare the purple and green lines in Fig. 7), which suggests that we can use the overturning split in pathways to get an impression of the importance of each route. In depth space, the maximum Eulerian (Lagrangian) overturning occurs at 1000 m depth and amounts to −3.8 (−4.1) Sv (Fig. 7b). Both *withinBC* and *interiorShort* particles contribute equally to the Lagrangian overturning in depth space. In addition, the presence of the *interiorLong* particles at the outflow becomes apparent in depths greater than 1000 m.

In density space, the overturning in both the Eulerian and Lagrangian view, peaks at a temperature of 3.5 °C and amounts to −3.4 and −5.4 Sv, respectively (Fig. 7d). When the contributions of the transport carried by each pathway to the net overturning in density space are considered, it appears that 60% of the maximum overturning (at T = 3.5 °C) can be attributed to the *interiorShort* particles and 40% to the *withinBC* particles. In contrast, the secondary peak of −4.1 Sv in the total Lagrangian overturning at T = 4.5 °C is mainly due to the *withinBC* particles. This confirms that the transformation of the *withinBC* particles results into relatively lighter water masses than the *interiorShort* particles. Notably, at this temperature, the Eulerian overturning is negligible. That is, the Eulerian transport of waters of this temperature at the inflow and outflow is the same, while the Lagrangian analysis reveals an increase in transport of this water mass. This implies that an inflow of waters of this temperature exists, which

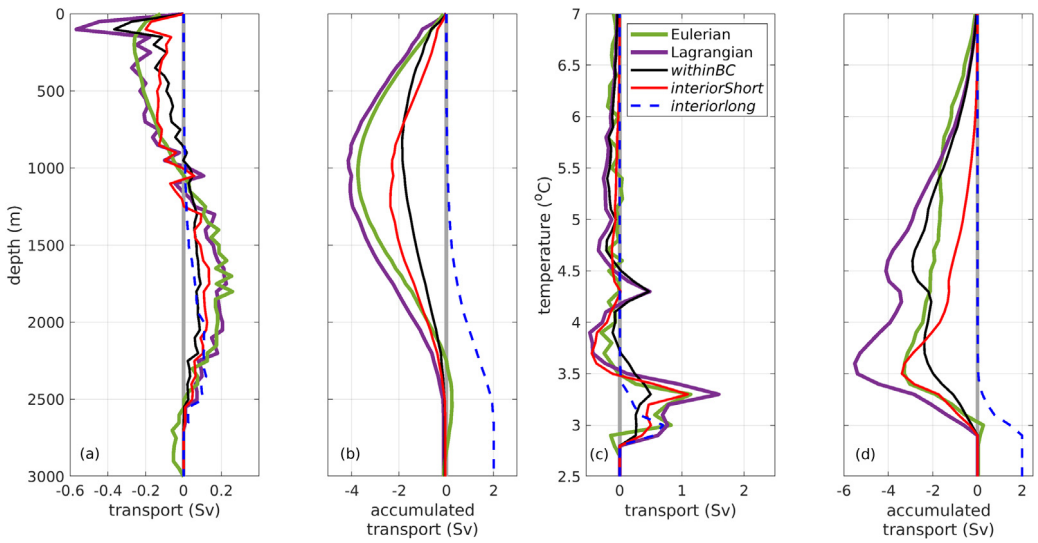

Fig. 7. Change of the volume transport (in Sv) between the outflow and inflow binned every (a) 50 m in depth and (c) 0.1 °C in temperature space for the annual mean Eulerian values (green line, mean over year 15; the particle release year), for the *withinBC* (black line), *interiorShort* (red line) particles and their sum (Lagrangian mean, purple line). Accumulated transport in (b) depth (shallow to deep) and (d) temperature (high to low) space. Also shown is the volume transport of the *interiorLong* particles at the outflow (blue dashed line).

does not reach the outflow within six years and is thus not captured by the Lagrangian backtracking calculation. The temperature of this water mass corresponds to that of boundary current waters at 500–1000 m depth (see Fig. 1b in Georgiou et al., 2019). We speculate that this water mass is also transported offshore from the boundary current to the interior, but has a residence time longer than the six-year duration of the Lagrangian calculation.

5. Subduction

As shown in Fig. 7, both the *withinBC* and the *interiorShort* particles experience water mass transformation. Here, we identify the location where these water masses last change their properties by means of the local subduction rate. Following the analysis of Brandt et al. (2007) we define subduction as the process of a particle leaving the mixed layer. It is calculated from the trajectories of the *withinBC* and *interiorShort* particles as the sum of all transport values assigned to the particles subducted within a certain grid box. The subduction velocity (Fig. 8) is calculated by dividing this subduction rate of each gridbox by its area. The magnitude of the subduction velocity is similar to the subduction velocities reported by Brandt et al. (2007) with elevated values in the west.

The calculation of the subduction rate is performed separately for the *withinBC* (Fig. 8a) and *interiorShort* particles (Fig. 8b). The main difference between the two is the location of the peak values: subduction of waters exiting the domain along the *withinBC* route mainly occurs in the western part of the Labrador Sea. This is likely associated with convection that occurs within the boundary current due to the surface buoyancy forcing. The total subduction of the *withinBC* particles amounts to 1.9 Sv. In contrast, large subduction velocities of the particles following the *interiorShort* route are found in the west, close to the edge of the boundary current. The total subduction for the *interiorShort* amounts to 3.7 Sv, of which 76% occurs in the interior (i.e. offshore of the 18 Sv contour line of Ψ_b). The remaining 24% subducts within the boundary current, after re-entering, which indicates a pathway of transformed water masses within the boundary current (Brandt et al., 2007) similar to the *withinBC* particles. Our study reveals that most of the *interiorShort* particles leave the mixed layer in the interior before they re-entrain into the boundary current and exit the domain (Fig. 8b). In the following section we will show that the properties of the particles depend on the location where they subduct within the interior (i.e., box 1 and box 2 in Fig. 8b).

6. Lateral exchange and water mass transformation

To explore the lateral exchange between the boundary current and the interior and water mass transformation in the interior, we next focus on the locations where the *interiorShort* particles enter and leave the interior of the domain. We define the first (last) crossing of a particle as the location at which it crosses the 18 Sv contour line of the barotropic streamfunction (Ψ_b) for the first (last) time after entering the domain (purple and yellow stars in the example trajectory shown in Fig. 2b).

An example trajectory shows that this particle enters the basin at the eastern open boundary at a depth of 100 m (Fig. 9c); its temperature at the inflow (green square in Fig. 9a) is T_{inflow} = 4.7 °C. It follows the boundary current until it crosses into the interior (purple star and vertical line in Fig. 9a and b, respectively). While in the interior, the particle recirculates and shows a large drop in temperature (Fig. 9b) when it is in the mixed layer (gray shaded area in Fig. 9b–c). There, it reaches a temperature corresponding to that of the convected water (T ~ 3.2 °C, Fig. 9b). Once the particle is subducted (Fig. 9c), it stays below the mixed layer in the subsequent winters and no further temperature change occurs (Fig. 9b). The largest change in depth of the particle (blue line in Fig. 9c) takes place between locations 5 and 6, when the particle leaves the mixed layer, without any water mass transformation. This means that the particle moves adiabatically along an isopycnal (isotherm) to deeper layers. For most of its advection time, the particle's path is steered by eddies that are present in the interior (Fig. 9a). After being in the interior for more than 4 years, the particle re-enters the boundary current (yellow star and vertical line in Fig. 9a-b) and it does so along this 3.2 °C isotherm. After its re-entry, the particle slightly rises in the water column (Fig. 9c) because the isotherms rise as the boundary current loses heat in the downstream direction (Straneo, 2006; Georgiou et al., 2019; Brüggemann and Katsman, 2019). Although it takes almost 6 years for this particle to travel from inflow to outflow, only nine months pass between the moment it re-enters the boundary current until it exits the Labrador Sea.

Next, we consider the lateral exchange between the boundary current and interior for all *interiorShort* and *interiorLong* particles. Most particles first cross into the interior at a distance between 380–850 km from the inflow (red dashed line, Fig. 10a). This peak in first crossings is found upstream of the peak in EKE along the boundary (~700 km downstream from the inflow, blue shading in Fig. 10a) associated with

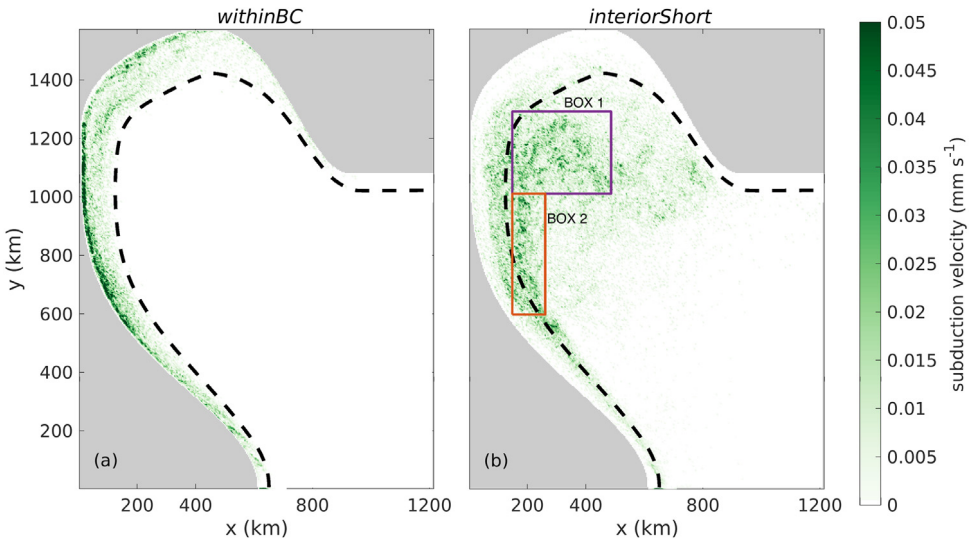

Fig. 8. Mean subduction velocity for (a) *withinBC* and (b) *interiorShort* particles. The black dashed line shows the 18 Sv barotropic streamfunction that is used to separate the particle pathways. Also included are the boxes in purple (box 1) and orange (box 2) indicating the regions of high subduction velocity that are used in the analysis in Section 6.

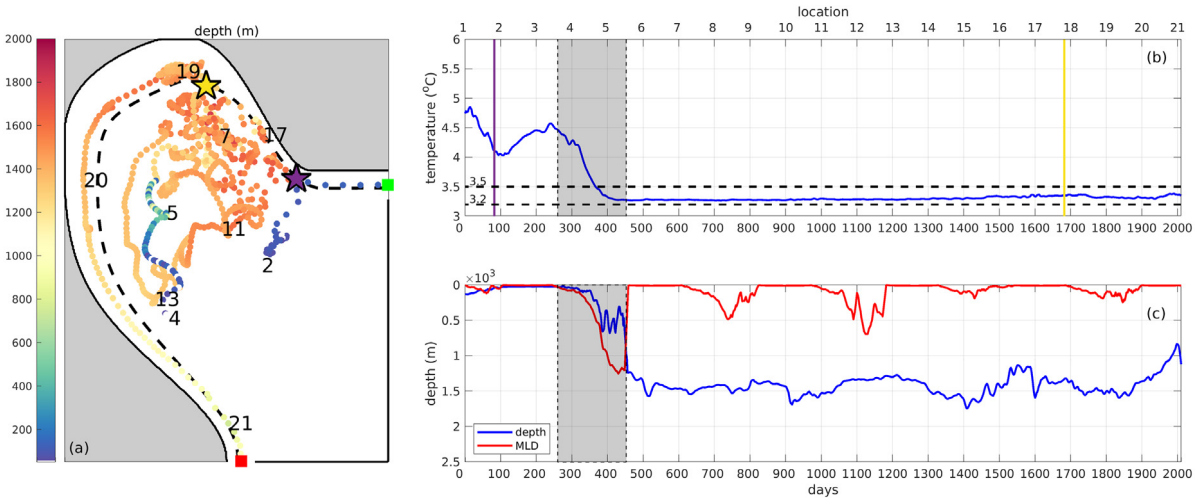

Fig. 9. (a) Example trajectory of an *interiorShort* particle. The particle's depth at each location is shown in color. Purple (yellow) star denotes the location of the first (last) crossing between boundary current and interior. Numbers correspond to time intervals of 100 days. (b–c) Time evolution of the particle's (b) temperature, (c) depth (blue line) and mixed layer depth at the particle's location (red line). Numbers on the top axis correspond to the location of the particle on the map in (a). The dashed horizontal lines in (b) show the temperature range of the product of convection in this idealized model (i.e. T = 3.2 – 3.5 °C) and the purple (yellow) vertical line denotes the moment of the first (last) crossing.

the eddy activity near the topographic narrowing (Fig. 1c). This is in agreement with the study of Schulze Chretien and Frajka-Williams (2018), who used Lagrangian trajectories to track the surface freshwater in the Labrador Sea and found that most of the freshwater leaves the shelf in the same area. This indicates that the topography plays a significant role in determining the interior–boundary current exchange: the enhanced EKE, due to enhanced eddy activity along the topographic narrowing (Figs. 1c and 10a) facilitates exchanges between the boundary current and the interior.

Most of the *interiorShort* particles also re-enter the boundary current in the area where EKE is enhanced (500–1000 km from the inflow, Fig. 10a); a secondary peak of last crossings is seen farther downstream coinciding with a secondary peak in EKE (distance ~2500 km). Similarly, the last crossings of the *interiorLong* particles (blue line in Fig. 10a) are also mostly found at the region of high EKE.

The average temperature of the particles entering the interior within 1000 km downstream of the inflow is 3.9 °C (dashed line in Fig. 10b). Notably, when they re-enter the boundary current, the particles are on average 0.2 °C colder (solid line). This corroborates that water mass transformation occurs during their time in the interior. At distances greater than 1500 km downstream of the inflow (i.e. the western side of the domain) the exchange occurs almost at the same temperature. This indicates that the boundary current-interior exchange at this part of the domain does not considerably affect the properties of the water masses. It is noteworthy that the *interiorLong* particles have a mean temperature of 3 °C or lower when they leave the interior (Fig. 10c), confirming once more that these particles represent the densest water mass in this model of the Labrador Sea.

To explore this connection in more detail, we now focus on the export routes of the water masses that have been subducted in the interior. We define two areas which represent regions of high subduction velocity (Fig. 8b) in box 1 and box 2, similarly to Brandt et al. (2007), and analyze only the behavior of the particles that subduct in these two boxes. So, the particles used for this analysis represent a fraction of the *interiorShort* particles (i.e. 20% of the particles, which represent 1.6 Sv or 43% of the total subduction in the interior). These boxes are placed in regions characterized by different dynamics: box 1 is located where the deepest mixed layers are found (Fig. 1b), while box 2 is placed near the Labrador coast where, accordingly to previous studies (e.g., Brandt et al., 2007), the newly-formed LSW is rapidly exported. It appears

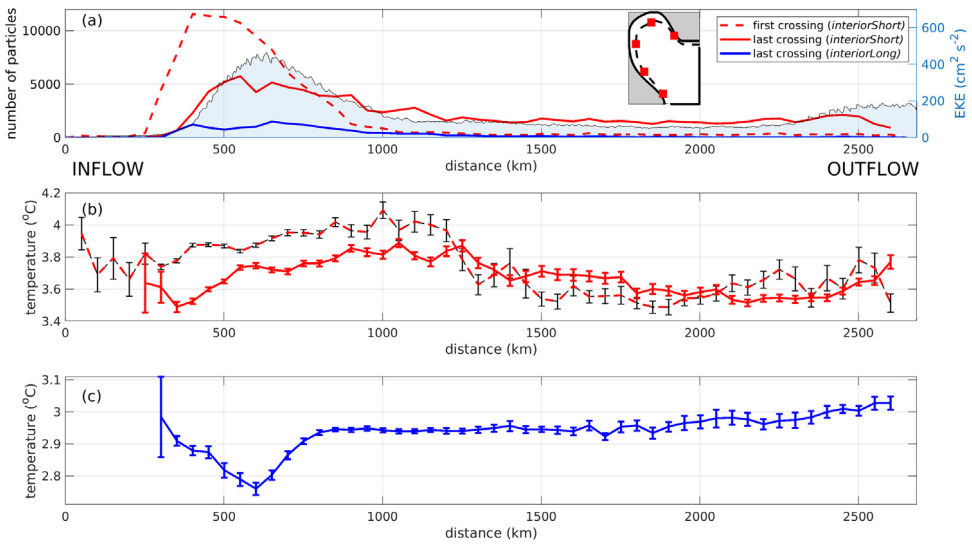

Fig. 10. (a) Number of particles and (b) mean temperature of particles at the first (dashed line) and last (solid line) crossings for the *interiorShort* particles. (c) As in (b) but for the *interiorLong* particles. Values are binned over segments of 50 km in alongshore direction (see inset, red circles mark distances every 500 km). The blue shaded area in (a) shows the EKE as a function of distance from the inflow. The error bars in (b–c) represent the 95% confidence interval of the mean values.

that the majority of the particles that subduct within box 1 (Fig. 11a) move towards the high EKE area near the Greenland coast (distance = 400–800 km) and re-enter the boundary current there before exiting the domain (purple line in Fig. 11c). In contrast, a large fraction of particles that subduct within box 2 (Fig. 11b) are directly entrained in the boundary current in the west (between 1600–2100 km, orange line in Fig. 11c). However, the number of particles subducted in box 2 is smaller than to the number that subducts in box 1 (i.e. 5643 particles difference that amounts to 0.5 Sv in terms of volume transport). This again explains the importance of the indirect export route via the West Greenland coast.

It is clear that the particles that subduct in box 1 and re-enter the boundary current where EKE peaks (distance between 400–1000 km) show a larger temperature change than the ones that subduct in box 2: they experience a mean cooling of $\Delta T_{box1}(400-1000\ \text{km}) = -0.5$ °C in contrast to $\Delta T_{box2}(400-1000\ \text{km}) = -0.2$ °C (Fig. 11d). This is due to the fact that the water masses subducted in these two boxes originate from different regions (Fig. 1b). In box 1, the mixed layer is deeper and temperatures are lower than in box 2. Essentially, Figs. 10b and 11d support the view that most of the *interiorShort* particles are transformed during their time in the interior. Moreover, depending on where water mass transformation occurs the particles tend to follow a different path and hence it is expected that they will display different residence times.

7. Residence time and export timescale

In this section, the residence time and export timescale of the particles are studied for each pathway. First, we investigate the residence time of the particles, defined as the time it takes a particle to travel from the inflow to the outflow. We focus on the *wholeLoop* particles, i.e. *withinBC* and *interiorShort* (Fig. 3), which all leave the basin within 6 years. It is clear that 90% of the *withinBC* particles leave the basin within one year (black bars in Fig. 12a); their maximum residence time is less than 2 years (black line in Fig. 12b). This highlights the existence of a fast route of water masses that enter the Labrador Sea and travel within the boundary current. As expected based on Fig. 9b, the *interiorShort* particles display much longer residence times of up to 6 years (Fig. 12a-b). However, 60% of the particles still leave the basin within 2 years (red line in Fig. 12b).

Next, we investigate if there is any connection between the properties of the water masses that exit the domain and their residence time in the basin by displaying the temperature of the particles at the outflow as a function of their residence time (Fig. 13). From this, it is evident that most of the *withinBC* particles (i.e. 60% of the particles, Fig. 13a) that leave the domain within one year correspond to lighter water masses ($T > 3.8$ °C). The residence time of the particles that exit the domain with temperatures lower than 3.8 °C is slightly longer but restricted to a maximum of 2 years. Here, the impact of the surface heat loss along the boundary in determining the properties of the local water mass is visible: the particles with $T < 3.8$ °C likely represent water masses formed during convection within the boundary current (Fig. 8a). Note that these particles are found deeper in the boundary current where its speed is weaker (Fig. 4), thus explaining their longer residence time. For the *interiorShort* particles the picture is different; 74% of the particles exits the domain with temperatures below 3.8 °C (Fig. 13b). Remarkably, the *interiorShort* particles that leave the basin within one year are particles that stay in the interior shortly and are warmer (i.e. $\bar{T}_{\text{residence<1year}} = 4$ °C). That is, the water masses that stay in the interior longer get denser (i.e. $\bar{T}_{\text{residence>1year}} = 3.6$ °C).

Besides the residence time, we also calculated the export timescale, defined as the time it takes a particle to reach the outflow after it has subducted. As expected, the export time for the *withinBC* particles is as expected very short: for 95% of the particles it is less than half a year. The export time of the *interiorShort* particles ranges from 4 days to 5.5 years. It appears that the water masses that are subducted within box 1 generally take more than one year before they exit the Labrador Sea; only 35% of the total transport carried by these particles is exported within one year. This is explained by the fact that the majority of these particles first moves towards the high EKE area near the Greenland coast before they re-enter the boundary current and reach the outflow (Fig. 11a). In contrast, the *interiorShort* particles that subduct in box 2 and are entrained into the boundary current in the west (Fig. 11b) exit the domain much quicker; 80% of the total transport carried by these particles is exported out of the Labrador Sea within 150 days.

8. Discussion and conclusions

In this study, the upstream pathways of the water masses exiting the Labrador Sea have been investigated from a Lagrangian perspective, with a focus on the exchange between the boundary current and the interior and the water mass transformation that occurs within the domain. To this end, the output of a regional idealized model is

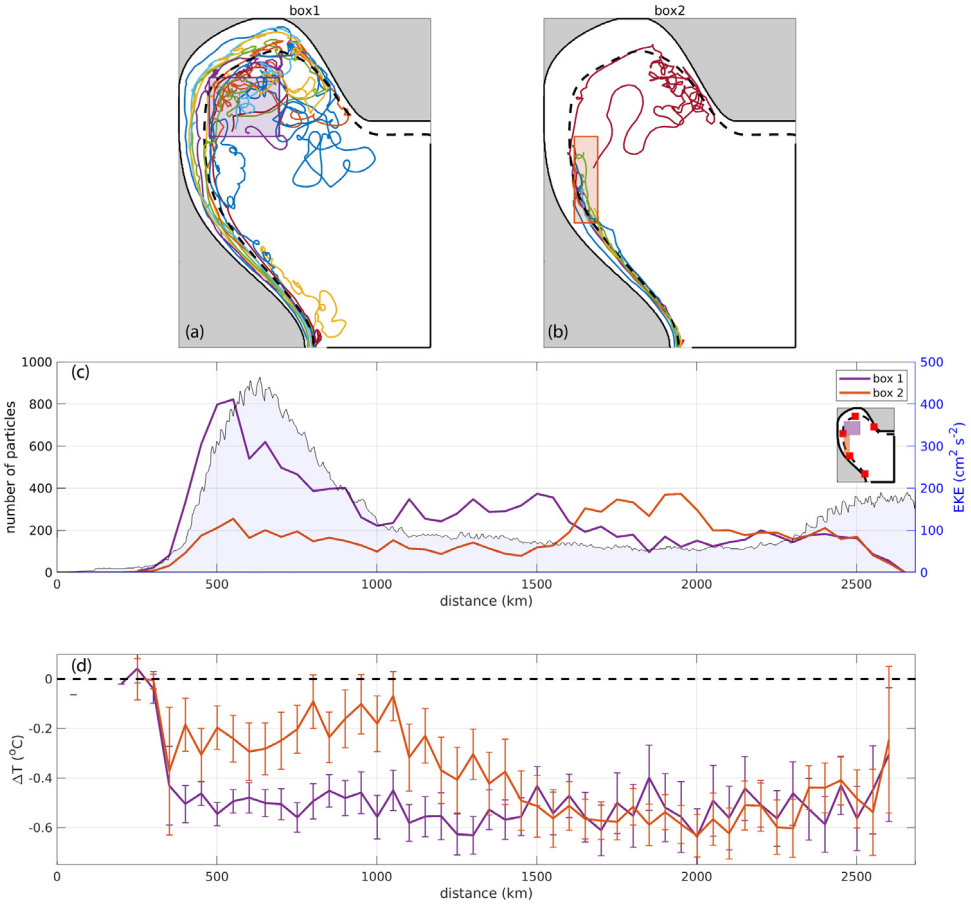

Fig. 11. Example trajectories from the location where the particles subduct in (a) box 1 (purple rectangle) and (b) box 2 (orange rectangle) to the outflow. (c) Number of particles that cross the 18 Sv contour for the last time and (d) mean temperature change (at the location of the last crossing) between the last and first crossing ($\Delta T = T_{last} - T_{first}$) as a function of distance from the inflow for the particles that subduct within box 1 (purple line) and box 2 (orange line). Values in (d) are binned over segments of 50 km in alongshore direction at the location of last crossing. The shaded area in (c) shows the EKE as a function of distance from the inflow (see inset, red squares mark distances every 500 km).

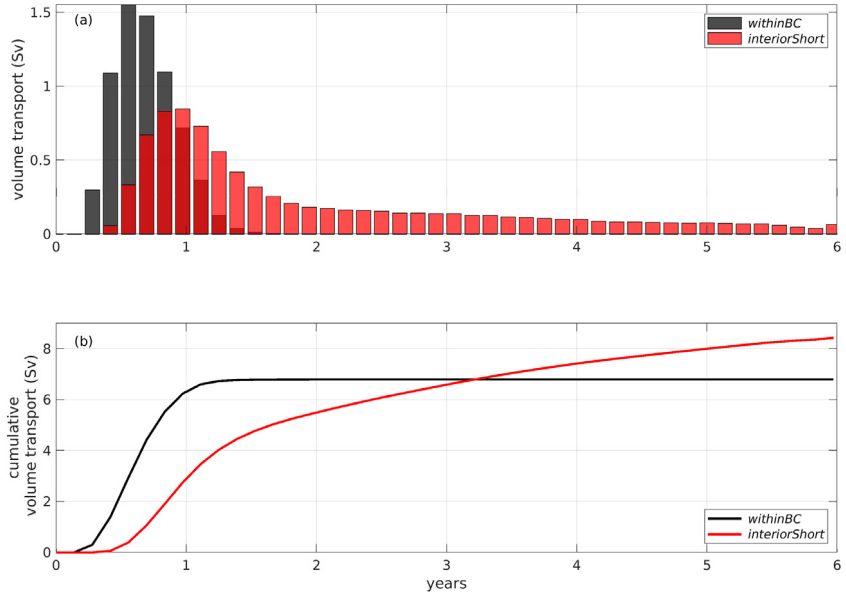

Fig. 12. (a) Volume transport and (b) cumulative volume transport of the *withinBC* (black bars/lines) and *interiorShort* (red bars/lines) particles, both as a function to their residence time (binned every 50 days) within the model domain.

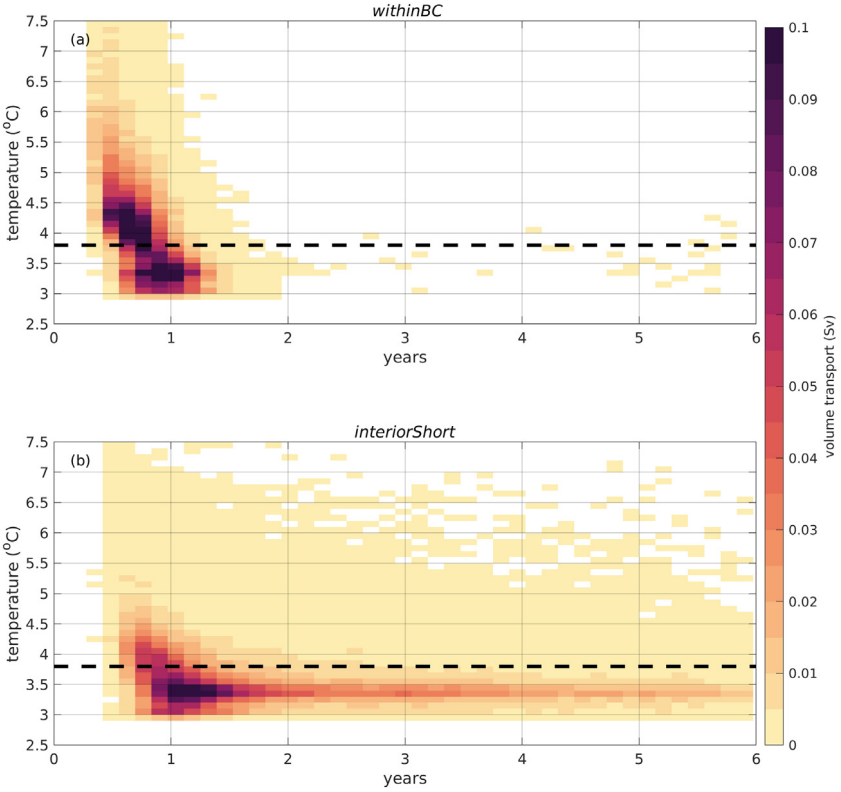

Fig. 13. Density distribution (in terms of volume transport) of the particle temperature at the outflow compared to the particle residence time for the particles that reach the outflow (*wholeLoop*) while (a) staying within the boundary current (*withinBC* particles) and (b) passing through the interior (*interiorShort* particles). The particle density is shown per ΔT = 0.1 °C and Δt = 50 days interval. The black dashed horizontal line shows the 3.8 °C isotherm.

used. This model is known to capture the mesoscale eddy activity in the Labrador Sea, which is most prominent at the West Greenland coast (Georgiou et al., 2019). The use of such an idealized model facilitates the exploration of the dynamics of this exchange between the boundary current and the interior and its role for LSW export. In this study, we extend the more generic study of a highly idealized marginal sea by Brüggemann and Katsman (2019), by quantifying the role of the interior–boundary exchanges in setting the properties and the associated timescales of the water masses exiting the marginal sea in more detail.

By assessing the processes from a Lagrangian viewpoint, we show that water masses follow either a direct route within the boundary current (*withinBC* particles) or an indirect route that involves boundary current-interior exchanges (*interiorShort* and *interiorLong* particles) from the inflow region south of Greenland to the outflow region on the Labrador side (Fig. 2b) that carry roughly the same transport. The distribution of the particles at the inflow and outflow (Fig. 4) shows that their position at the inflow determines their pathway and location at the outflow. Essentially, the particles that follow the boundary current (*withinBC*) are found in the core of the boundary current with rather high velocities, while particles that pass through the interior (*interiorShort*) are found on its outer flank. That is, our results indicate that the fate of water masses is already determined upstream. This suggests that processes in the Irminger Basin and Nordic Seas impact the water mass transformation in the Labrador Sea.

Building on the generic idea proposed by Brüggemann and Katsman (2019) on the existence of a fast and a slow route for dense water masses that exit the Labrador Sea, the Lagrangian analysis presented in this study allows us to quantify the transports associated with those two pathways. The depth change of the particles between the inflow and outflow reveals that the total volume transport between 1500–3000 m increases by 1.3 Sv for the *withinBC* particles and by 2.0 Sv for the *interiorShort* particles (Fig. 5). In density space (which in this idealized model is represented by temperature only), the Lagrangian trajectories also show a substantial transport change between the inflow and outflow through the 3.5 °C isotherm which amounts to 2.2 Sv and 3.4 Sv for the *withinBC* and *interiorShort* particles, respectively (Fig. 6). The maximum overturning derived from the Eulerian quantities amounts to −3.8 Sv at 1000 m (depth space, Fig. 7b) and −3.4 Sv at 3.5 °C (density space, Fig. 7d). The Lagrangian particles capture the net Eulerian overturning observed in this model both in depth and density space well (Fig. 7), considering the fact that not all the particle trajectories cover the entire path between in- and outflow. The relative importance of the different pathways on the overturning becomes apparent in density space; 60% of the maximum overturning is related to the transport carried by the *interiorShort* particles and only 40% by the *withinBC* particles (Fig. 7c-d). However, there is also a significant signal in the overturning in lighter layers, which is only related to the relatively slow moving fraction of the *withinBC* particles. In short, the volume transport of the densest water masses is primarily carried by particles that have resided in the interior (i.e. *interiorShort* and *interiorLong* particles), while the particles that follow the fast route (i.e. *withinBC*) mainly transform in lighter water masses.

The characteristics of water mass transformation also differ for the fast and slow pathways. The *withinBC* particles mainly subduct on the southwest side of the Labrador Sea (Fig. 8a). This location is downstream of the region where strong surface heat loss has reduced the stratification of the boundary current, allowing the water masses to be transformed into denser water masses. In contrast, the *interiorShort* particles generally enter the interior at the Greenland side (Fig. 10a), experience water mass transformation in the interior at the convection region (Figs. 8b and 10b), before re-entering the boundary current (Fig. 10). The latter occurs predominantly on the Greenland side and to a lesser extent on the Labrador side (Fig. 10a), depending on the location where the particle last leaves the mixed layer (Fig. 11). This two-way exchange (first and last crossings) at the western coast of

Greenland has been also identified in the recent study of Pennelly et al. (2019). However, our study highlights that the export of the water masses that have been transformed into denser water masses in the interior occurs laterally, as they are advected towards the region of high EKE on the Greenland side by eddy stirring.

The exchange between the boundary current and the interior has a direct impact on the timescales of the export of the water masses (Fig. 13): 90% of the volume transport carried by the *withinBC* particles exits the basin within one year, while only 30% of the transport associated with the *interiorShort* particles exits within that time frame. In observations (Bower et al., 2009) and models (Brandt et al., 2007; Feucher et al., 2019) the newly formed LSW is exported within one year. Our Lagrangian analysis supports the idea of previous observational studies that the quickly exported LSW is likely formed within or close to the boundary current (Pickart et al., 2002; Cuny et al., 2005). Most of the *interiorLong* particles also re-enter the boundary current at the region of high EKE (Fig. 10c). However, due to topographic constraints the lateral, along isopycnal transport towards the boundary current at the high EKE region cannot as easily take place for the denser *interiorLong* as for the lighter *interiorShort* particles. This results in a longer residence of the *interiorLong* particles within the interior. Essentially, the fact that the densest water masses, which are represented by the *interiorLong* particles, take more than six years to fully pass through the Labrador Sea, confirms that cold signals that are exported from the Labrador Sea do not need to correspond to recent convective events, as suggested by Cuny et al. (2005). Thus, our results suggest that the observed year-to-year correspondence between the properties of the water masses found in the interior of the Labrador Sea and in the Labrador Current (e.g., Rhein et al., 2015; Yashayaev and Loder, 2016; Holte and Straneo, 2017; Le Bras et al., 2017) reflect variations of the fast export route of LSW formed close to or within the boundary current.

Our Lagrangian results clearly extend the tracer analysis performed by Georgiou et al. (2019) and Brüggemann and Katsman (2019), as these studies mostly provided a qualitative description of the connection between strong eddy activity and convection areas. The Lagrangian analysis using particles instead of a passive tracer allows for conditional analysis (see van Sebille et al., 2018) and provides a quantification of the relative importance of each pathway to water mass transformation and to the overturning in depth and density space.

In our study, the limited model domain does not allow the investigation of the export route towards the Irminger Sea discussed in Section 1 (e.g., Lavender et al., 2000; Pickart et al., 2003). Therefore, our results may overestimate the transport of the LSW towards the West Greenland coast. Another aspect that cannot be covered in our idealized model simulation but deserves attention is the suggestion by Lozier et al. (2013) that the overflow waters entering the subpolar gyre from the Nordic Seas also follow interior pathways that substantially lead to their equatorward export through the Labrador Sea. We expect a minimal transformation of the overflow waters within the Labrador Sea since they fill the deeper layers of the basin. However, the presence of the overflow waters may affect the LSW pathways. Nevertheless, the conclusion that an eddy driven transport of dense water towards the boundary exists and that it affects the export timescales of LSW is expected to hold. Analyses with a more realistic high-resolution model are needed to explore this in more detail.

One of the main findings of this study is that there is a fast, direct route for relatively lighter water masses compared to the slower, indirect route that the denser water masses follow to exit the Labrador Sea. In this model, both routes carry roughly the same transport, but the indirect route is steered by the eddy activity near the Greenland coast. That is, a preferable region for lateral spreading of LSW and entrainment in the boundary current is identified. Therefore, the view of a homogeneous lateral spreading and entrainment of the LSW into the boundary current is not valid in our model, and this is consistent with the studies of Bower et al. (2009, 2011) and Gary et al. (2012). Importantly, the fact that the densest water masses found in this study take more than six years to exit the Labrador Sea might obscure the link between the LSW formation and AMOC variability in observations such as the OSNAP array (Holliday et al., 2018; Lozier et al., 2019).

The result that the interior–boundary current exchange is important for the LSW export and hence contributes to the AMOC variability, suggests that additional observations aimed at capturing these mechanisms are needed. It also raises the question how well LSW export processes, their variability and their relation to AMOC variability are represented in climate models, which lack the resolution to resolve the mesoscale features required to capture this interior–boundary current exchange.

Declaration of competing interest

The authors declare that they have no known competing financial interests or personal relationships that could have appeared to influence the work reported in this paper.

CRediT authorship contribution statement

Sotiria Georgiou: Conceptualization, Investigation, Methodology, Software, Formal analysis, Visualization, Writing - original draft. **Stefanie L. Ypma:** Methodology, Software, Writing - review & editing. **Nils Brüggemann:** Methodology, Software, Writing - review & editing. **Juan-Manuel Sayol:** Methodology, Writing - review & editing. **Julie D. Pietrzak:** Supervision, Writing - review & editing. **Caroline A. Katsman:** Funding acquisition, Supervision, Conceptualization, Methodology, Writing - review & editing.

Acknowledgments

S. Georgiou, S.L. Ypma, and J.-M. Sayol were supported by the Netherlands Organisation for Scientific Research (NWO) via VIDI grant 864.13.011 awarded to C. A. Katsman. N. Brüggemann was also funded by the Collaborative Research Centre, The Netherlands TRR 181. This paper is a contribution to the project S2 (Improved parameterisations and numerics in climate models) of the Collaborative Research Centre TRR 181 “Energy Transfer in Atmosphere and Ocean” funded by the Deutsche Forschungsgemeinschaft (DFG, German Research Foundation, Germany) - Projektnummer 274762653. Comments from C.G. van der Boog on the analysis and the insightful comments and suggestions of two anonymous reviewers are greatly appreciated. The model data analyzed in this study are available from the corresponding author on request.

References

Biastoch, A., Böning, C.W., Getzlaff, J., Molines, J.-M., Madec, G., 2008. Causes of Interannual–Decadal Variability in the Meridional Overturning Circulation of the Midlatitude North Atlantic Ocean. J. Clim. 21 (24), 6599–6615. http://dx.doi.org/10.1175/2008JCLI2404.1.

Bower, A., Lozier, S., Biastoch, A., Drouin, K., Foukal, N., Furey, H., Lankhorst, M., Rühs, S., Zou, S., 2019. Lagrangian Views of the Pathways of the Atlantic Meridional Overturning Circulation. J. Geophys. Res.: Oceans 124, http://dx.doi.org/10.1029/2019JC015014.

Bower, A., Lozier, S., Gary, S., 2011. Export of Labrador Sea Water from the subpolar North Atlantic: A Lagrangian perspective. Deep Sea Res. Part II 58 (17), 1798–1818. http://dx.doi.org/10.1016/j.dsr2.2010.10.060.

Bower, A.S., Lozier, M.S., Gary, S.F., Böning, C.W., 2009. Interior pathways of the North Atlantic meridional overturning circulation. Nature 459, 243–247. http://dx.doi.org/10.1038/nature07979.

Brandt, P., Funk, A., Czeschel, L., Eden, C., Böning, C.W., 2007. Ventilation and Transformation of Labrador Sea Water and Its Rapid Export in the Deep Labrador Current. J. Phys. Oceanogr. 37 (4), 946–961. http://dx.doi.org/10.1175/JPO3044.1.

Brüggemann, N., Katsman, C.A., 2019. Dynamics of downwelling in an eddying marginal sea: contrasting the Eulerian and the isopycnal prespective. J. Phys. Oceanogr. http://dx.doi.org/10.1175/JPO-D-19-0090.1.

Collins, M., Knutti, R., Arblaster, J., Dufresne, J.-L., Fichefet, T., Friedlingstein, P., Gao, X., Gutowski, W.J., Johns, T., Krinner, G., Shongwe, M., Tebaldi, C., Weaver, A.J., Wehner, M., 2013. Long-term Climate Change: Projections, Commitments and Irreversibility Pages 1029 to 1076. In: Intergovernmental Panel on Climate Change (Ed.), Climate Change 2013 - the Physical Science Basis. Cambridge University Press, Cambridge, pp. 1029–1136. http://dx.doi.org/10.1017/CBO9781107415324.024.

Cunningham, S.A., Kanzow, T., Rayner, D., Baringer, M.O., Johns, W.E., Marotzke, J., Longworth, H.R., Grant, E.M., Hirschi, J.J.-M., Beal, L.M., Meinen, C.S., Bryden, H.L., 2007. Temporal Variability of the Atlantic Meridional Overturning Circulation at 26.5° N. Science 317 (5840), 935–938. http://dx.doi.org/10.1126/science.1141304.

Cuny, J., Rhines, P.B., Schott, F., Lazier, J., 2005. Convection above the Labrador Continental Slope. J. Phys. Oceanogr. 35 (4), 489–511. http://dx.doi.org/10.1175/JPO2700.1.

de Jong, M.F., Bower, A.S., Furey, H.H., 2016. Seasonal and Interannual Variations of Irminger Ring Formation and Boundary-Interior Heat Exchange in FLAME. J. Phys. Oceanogr. 46 (6), 1717–1734. http://dx.doi.org/10.1175/jpo-d-15-0124.1.

Desbruyères, D.G., Mercier, H., Maze, G., Daniault, N., 2019. Surface predictor of overturning circulation and heat content change in the subpolar North Atlantic. Ocean Sci. 15 (3), 809–817. http://dx.doi.org/10.5194/os-15-809-2019.

Döös, K., 1995. Interocean exchange of water masses. J. Geophys. Res.: Oceans 100 (C7), 13499–13514. http://dx.doi.org/10.1029/95JC00337.

Feucher, C., Garcia-Quintana, Y., Yashayaev, I., Hu, X., Myers, P.G., 2019. Labrador Sea Water formation rate and its impact on the local Meridional Overturning Circulation. J. Geophys. Res.: Oceans http://dx.doi.org/10.1029/2019JC015065.

Fischer, J., Schott, F.A., Dengler, M., 2004. Boundary Circulation at the Exit of the Labrador Sea. J. Phys. Oceanogr. 34 (7), 1548–1570. http://dx.doi.org/10.1175/1520-0485(2004)034<1548:BCATEO>2.0.CO;2.

Gary, S.F., Lozier, M.S., Biastoch, A., Böning, C.W., 2012. Reconciling tracer and float observations of the export pathways of Labrador Sea Water. Geophys. Res. Lett. 39 (24), http://dx.doi.org/10.1029/2012GL053978.

Gelderloos, R., Katsman, C.A., Drijfhout, S.S., 2011. Assessing the Roles of Three Eddy Types in Restratifying the Labrador Sea after Deep Convection. J. Phys. Oceanogr. 41 (11), 2102–2119. http://dx.doi.org/10.1175/JPO-D-11-054.1.

Gelderloos, R., Straneo, F., Katsman, C.A., 2012. Mechanisms behind the Temporary Shutdown of Deep Convection in the Labrador Sea: Lessons from the Great Salinity Anomaly Years 1968–71. J. Clim. 25 (19), 6743–6755. http://dx.doi.org/10.1175/JCLI-D-11-00549.1.

Georgiou, S., van der Boog, C.G., Brüggemann, N., Ypma, S.L., Pietrzak, J.D., Katsman, C.A., 2019. On the interplay between downwelling, deep convection and mesoscale eddies in the Labrador Sea. Ocean Model. 135, 56–70. http://dx.doi.org/10.1016/j.ocemod.2019.02.004.

Holliday, N.P., Bacon, S., Allen, J., McDonagh, E.L., 2009. Circulation and Transport in the Western Boundary Currents at Cape Farewell, Greenland. J. Phys. Oceanogr. 39 (8), 1854–1870. http://dx.doi.org/10.1175/2009JPO4160.1.

Holliday, N.P., Bacon, S., Cunningham, S.A., Gary, S.F., Karstensen, J., King, B.A., Li, F., Mcdonagh, E.L., 2018. Subpolar North Atlantic Overturning and Gyre-Scale Circulation in the Summers of 2014 and 2016. J. Geophys. Res.: Oceans 123 (7), 4538–4559. http://dx.doi.org/10.1029/2018JC013841.

Holte, J., Straneo, F., 2017. Seasonal Overturning of the Labrador Sea as Observed by Argo Floats. J. Phys. Oceanogr. 47 (10), 2531–2543. http://dx.doi.org/10.1175/JPO-D-17-0051.1.

Johnson, H.L., Cessi, P., Marshall, D.P., Schloesser, F., Spall, M.A., 2019. Recent Contributions of Theory to Our Understanding of the Atlantic Meridional Overturning Circulation. J. Geophys. Res.: Oceans 124 (8), 5376–5399. http://dx.doi.org/10.1029/2019JC015330.

Katsman, C.A., Spall, M.A., Pickart, R.S., 2004. Boundary Current Eddies and Their Role in the Restratification of the Labrador Sea*. J. Phys. Oceanogr. 34 (9), 1967–1983. http://dx.doi.org/10.1175/1520-0485(2004)034<1967:BCEATR>2.0.CO;2.

Khatiwala, S., Visbeck, M., 2000. An estimate of the eddy-induced circulation in the Labrador Sea. Geophys. Res. Lett. 27 (15), 2277–2280. http://dx.doi.org/10.1029/1999GL011073.

Kulan, N., Myers, P.G., 2009. Comparing two climatologies of the Labrador Sea: Geopotential and isopycnal. Atmos.-Ocean 47 (1), 19–39. http://dx.doi.org/10.3137/OC281.2009.

Lavender, K., Davis, R., Owens, W., 2000. Mid-depth recirculation observed in the interior Labrador and Irminger seas by direct velocity measurements. Nature 407 (6800), 66–69. http://dx.doi.org/10.1038/35024048.

Le Bras, I.A., Yashayaev, I., Toole, J.M., 2017. Tracking Labrador Sea Water property signals along the Deep Western Boundary Current. J. Geophys. Res.: Oceans 122 (7), 5348–5366. http://dx.doi.org/10.1002/2017JC012921.

Li, F., Lozier, M.S., 2018. On the Linkage between Labrador Sea Water Volume and Overturning Circulation in the Labrador Sea: A Case Study on Proxies. J. Clim. 31 (13), 5225–5241. http://dx.doi.org/10.1175/JCLI-D-17-0692.1.

Li, F., Lozier, M.S., Johns, W.E., 2017. Calculating the Meridional Volume, Heat, and Freshwater Transports from an Observing System in the Subpolar North Atlantic: Observing System Simulation Experiment. J. Atmos. Ocean. Technol. 34 (7), 1483–1500. http://dx.doi.org/10.1175/JTECH-D-16-0247.1.

Lozier, M.S., Gary, S.F., Bower, A.S., 2013. Simulated pathways of the overflow waters in the North Atlantic: Subpolar to subtropical export. Deep Sea Res. Part II 85, 147–153. http://dx.doi.org/10.1016/j.dsr2.2012.07.037.

Lozier, M.S., Li, F., Bacon, S., Bahr, F., Bower, A.S., Cunningham, S.A., de Jong, M.F., de Steur, L., deYoung, B., Fischer, J., Gary, S.F., Greenan, B.J.W., Holliday, N.P., Houk, A., Houpert, L., Inall, M.E., Johns, W.E., Johnson, H.L., Johnson, C., Karstensen, J., Koman, G., Le Bras, I.A., Lin, X., Mackay, N., Marshall, D.P., Mercier, H., Oltmanns, M., Pickart, R.S., Ramsey, A.L., Rayner, D., Straneo, F., Thierry, V., Torres, D.J., Williams, R.G., Wilson, C., Yang, J., Yashayaev, I., Zhao, J., 2019. A sea change in our view of overturning in the subpolar North Atlantic. Science 363 (6426), 516–521. http://dx.doi.org/10.1126/science.aau6592.

Marshall, J., Adcroft, A., Hill, C., Perelman, L., Heisey, C., 1997. A finite-volume, incompressible Navier Stokes model for studies of the ocean on parallel computers. J. Geophys. Res. 102 (C3), 5753–5766. http://dx.doi.org/10.1029/96JC02775.

Palter, J.B., Lozier, M.S., Lavender, K.L., 2008. How Does Labrador Sea Water Enter the Deep Western Boundary Current? J. Phys. Oceanogr. 38 (5), 968–983. http://dx.doi.org/10.1175/2007JPO3807.1.

Paris, C.B., Helgers, J., van Sebille, E., Srinivasan, A., 2013. Connectivity Modeling System: A probabilistic modeling tool for the multi-scale tracking of biotic and abiotic variability in the ocean. Environ. Model. Softw. 42, 47–54. http://dx.doi.org/10.1016/j.envsoft.2012.12.006.

Pennelly, C., Hu, X., Myers, P.G., 2019. Cross-Isobath Freshwater Exchange Within the North Atlantic Subpolar Gyre. J. Geophys. Res.: Oceans 124 (10), 6831–6853. http://dx.doi.org/10.1029/2019JC015144.

Pickart, R.S., Straneo, F., Moore, G., 2003. Is Labrador Sea Water formed in the Irminger basin? Deep Sea Res. Part I 50 (1), 23–52. http://dx.doi.org/10.1016/S0967-0637(02)00134-6.

Pickart, R.S., Torres, D.J., Clarke, R.A., 2002. Hydrography of the Labrador Sea during Active Convection. J. Phys. Oceanogr. 32 (2), 428–457. http://dx.doi.org/10.1175/1520-0485(2002)032<0428:HOTLSD>2.0.CO;2.

Rhein, M., Kieke, D., Steinfeldt, R., 2015. Advection of North Atlantic Deep Water from the Labrador Sea to the southern hemisphere. J. Geophys. Res.: Oceans 120 (4), 2471–2487. http://dx.doi.org/10.1002/2014JC010605.

Rhein, M., Steinfeldt, R., Kieke, D., Stendardo, I., Yashayaev, I., 2017. Ventilation variability of Labrador Sea Water and its impact on oxygen and anthropogenic carbon: a review. Phil. Trans. R. Soc. A 375 (2102), http://dx.doi.org/10.1098/rsta.2016.0321.

Rykova, T., Straneo, F., Bower, A.S., 2015. Seasonal and interannual variability of the West Greenland Current System in the Labrador Sea in 1993-2008. J. Geophys. Res.: Oceans 120 (2), 1318–1332. http://dx.doi.org/10.1002/2014JC010386.

Schulze Chretien, L.M., Frajka-Williams, E., 2018. Wind-driven transport of fresh shelf water into the upper 30m of the Labrador Sea. Ocean Sci. 14 (5), 1247–1264. http://dx.doi.org/10.5194/os-14-1247-2018.

van Sebille, E., Griffies, S.M., Abernathey, R., Adams, T.P., Berloff, P., Biastoch, A., Blanke, B., Chassignet, E.P., Cheng, Y., Cotter, C.J., Deleersnijder, E., Döös, K., Drake, H.F., Drijfhout, S., Gary, S.F., Heemink, A.W., Kjellsson, J., Koszalka, I.M., Lange, M., Lique, C., MacGilchrist, G.A., Marsh, R., Adame, C.G.M., McAdam, R., Nencioli, F., Paris, C.B., Piggott, M.D., Polton, J.A., Rühs, S., Shah, S.H., Thomas, M.D., Wang, J., Wolfram, P.J., Zanna, L., Zika, J.D., 2018. Lagrangian ocean analysis: Fundamentals and practices. Ocean Model. 121, 49–75. http://dx.doi.org/10.1016/j.ocemod.2017.11.008.

van Sebille, E., Spence, P., Mazloff, M.R., England, M.H., Rintoul, S.R., Saenko, O.A., 2013. Abyssal connections of Antarctic Bottom Water in a Southern Ocean State Estimate. Geophys. Res. Lett. 40 (10), 2177–2182. http://dx.doi.org/10.1002/grl.50483.

Smeed, D.A., Josey, S.A., Beaulieu, C., Johns, W.E., Moat, B.I., Frajka-Williams, E., Rayner, D., Meinen, C.S., Baringer, M.O., Bryden, H.L., McCarthy, G.D., 2018. The North Atlantic Ocean Is in a State of Reduced Overturning. Geophys. Res. Lett. 45 (3), 1527–1533. http://dx.doi.org/10.1002/2017GL076350.

Stramma, L., Kieke, D., Rhein, M., Schott, F., Yashayaev, I., Koltermann, K.P., 2004. Deep water changes at the western boundary of the subpolar North Atlantic during 1996 to 2001. Deep Sea Res. Part I 51 (8), 1033–1056. http://dx.doi.org/10.1016/j.dsr.2004.04.001.

Straneo, F., 2006. On the Connection between Dense Water Formation, Overturning, and Poleward Heat Transport in a Convective Basin*. J. Phys. Oceanogr. 36 (9), 1822–1840. http://dx.doi.org/10.1175/JPO2932.1.

Straneo, F., Pickart, R.S., Lavender, K., 2003. Spreading of Labrador sea water: an advective-diffusive study based on Lagrangian data. Deep-Sea Res. Part I 50 (6), 701–719. http://dx.doi.org/10.1016/S0967-0637(03)00057-8.

Talley, L.D., McCartney, M.S., 1982. Distribution and Circulation of Labrador Sea Water. J. Phys. Oceanogr. 12 (11), 1189–1205. http://dx.doi.org/10.1175/1520-0485(1982)012<1189:DACOLS>2.0.CO;2.

Weijer, W., Cheng, W., Drijfhout, S.S., Fedorov, A.V., Hu, A., Jackson, L.C., Liu, W., McDonagh, E.L., Mecking, J.V., Zhang, J., 2019. Stability of the Atlantic Meridional Overturning Circulation: A Review and Synthesis. J. Geophys. Res.: Oceans 124 (8), 5336–5375. http://dx.doi.org/10.1029/2019JC015083.

Wunsch, C., Heimbach, P., 2006. Estimated Decadal Changes in the North Atlantic Meridional Overturning Circulation and Heat Flux 1993–2004. J. Phys. Oceanogr. 36 (11), 2012–2024. http://dx.doi.org/10.1175/JPO2957.1.

Xu, X., Rhines, P.B., Chassignet, E.P., 2016. Temperature-salinity structure of the North Atlantic circulation and associated heat and freshwater transports. J. Clim. 29 (21), 7723–7742. http://dx.doi.org/10.1175/JCLI-D-15-0798.1.

Yashayaev, I., Loder, J.W., 2016. Further intensification of deep convection in the Labrador Sea in 2016. Geophys. Res. Lett. 44 (3), 1429–1438. http://dx.doi.org/10.1002/2016GL071668.

Yeager, S., Danabasoglu, G., 2014. The Origins of Late-Twentieth-Century Variations in the Large-Scale North Atlantic Circulation. J. Clim. 27 (9), 3222–3247. http://dx.doi.org/10.1175/JCLI-D-13-00125.1.

Ypma, S., Brüggemann, N., Georgiou, S., Spence, P., Dijkstra, H., Pietrzak, J., Katsman, C., 2019. Pathways and watermass transformation of Atlantic Water entering the Nordic Seas through Denmark Strait in two high resolution ocean models. Deep Sea Res. Part I 145, 59–72. http://dx.doi.org/10.1016/j.dsr.2019.02.002.

Zhang, R., 2010. Latitudinal dependence of Atlantic meridional overturning circulation (AMOC) variations. Geophys. Res. Lett. 37 (16), http://dx.doi.org/10.1029/2010GL044474.

Zou, S., Lozier, M.S., 2016. Breaking the Linkage Between Labrador Sea Water Production and Its Advective Export to the Subtropical Gyre. J. Phys. Oceanogr. 46 (7), 2169–2182. http://dx.doi.org/10.1175/JPO-D-15-0210.1.